JACS
JOURNAL OF THE AMERICAN CHEMICAL SOCIETY
Article
pubs.acs.org/JACS

Revealing the Origin of Fast Electron Transfer in TiO_2-Based Dye-Sensitized Solar Cells

Hai Wei,[†,‡,∥] Jun-Wei Luo,[*,†,‡,∥] Shu-Shen Li,[†,‡,∥] and Lin-Wang Wang[*,§]

[†]State Key Laboratory of Superlattices and Microstructures, Institute of Semiconductors, Chinese Academy of Sciences, P.O. Box 912, Beijing 100083, China

[‡]University of Chinese Academy of Sciences, Beijing 100049, China

[∥]Synergetic Innovation Center of Quantum Information and Quantum Physics, University of Science and Technology of China, Hefei, Anhui 230026, China

[§]Materials Science Division, Lawrence Berkeley National Laboratory, Berkeley, California 94720, United States

Supporting Information

ABSTRACT: In dye-sensitized solar cells (DSCs), the electron transfer from photoexcited dye molecules to semiconductor substrates remains a major bottleneck. Replacing TiO_2 with ZnO is expected to enhance the efficiency of DSCs, owing to the latter possesses a much larger electron mobility, but similar bandgap and band positions as TiO_2 remain. However, the record efficiency of ZnO-based DSCs is only 7% compared with 13% of TiO_2-based DSCs due to the even slower electron-transfer rate in ZnO-based DSCs, which becomes a long-standing puzzle. Here, we computationally investigate the electron transfer from the dye molecule into ZnO and TiO_2, respectively, by performing the first-principles calculations within the frame of the Marcus theory. The predicted electron-transfer rate in the TiO_2-based DSC is about 1.15×10^9 s^{-1}, a factor of 15 faster than that of the ZnO-based DSC, which is in good agreement with experimental data. We find that the much larger density of states of the TiO_2 compared with ZnO near the conduction band edge is the dominant factor, which is responsible for the faster electron-transfer rate in TiO_2-based DSCs. These denser states provide additional efficient channels for the electron transfer. We also provide design principles to boost the efficiency of DSCs through surface engineering of high mobility photoanode semiconductors.

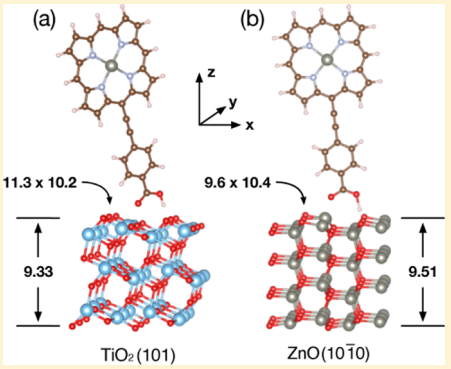

INTRODUCTION

O'Regan and Grätzel in their seminal work proposed the prototype of dye-sensitized solar cells (DSCs)[1] and provided an alternative concept to traditional p−n junction solar cells. A DSC contains three main components: dye molecules used as the light absorber, wide bandgap semiconductor served dual functions as the support for dye loading and transporter of photoexcited electrons from dye molecules to the electrode, and the redox hole shuttle. The dye molecules anchor on the surface of the wide-bandgap semiconductor such as TiO_2, ZnO, or SnO_2.[2] Once the dye molecule absorbs a photon and then generates an electron−hole pair, the photoexcited electron transfers rapidly to the conduction band minimum (CBM) of the semiconductor, which carries the electron to one of the electrodes. The redox couple, immersed in the electrolyte, takes away the remaining hole from the dye molecule and transports it to the counter-electrode. Therefore, the electron transfer (ET) from photoexcited dye molecules to semiconductor substrates in DSCs is required to be sufficiently fast to compete effectively against carrier loss processes in order to achieve high conversion efficiencies. DSCs possess striking advantages over the conventional crystalline silicon solar cells, which dominate the solar cell industry with about 89% of the market. The most attractive properties of DSCs are their low production costs, simple fabrication, and tunable optical properties. After more than 20 years of research, the DSCs have been developed into a major interest in the field of photovoltaics.[2]

In order to improve the efficiency of DSCs, experimental groups all over the world have examined thousands of dye/semiconductor/redox combinations.[3] For the part of light-sensitized dye, the polypyridyl dye molecules based on the ruthenium (Ru) are widely studied.[4,5] Other dyes such as porphyrin[6−8] are also investigated as promising candidates. The strategy on optimizing the dyes is to cover wider spectral or enhance the light extinction coefficient.[5,7,9] For the part of redox, iodide/triiodide(I^-/I_3^-) is most successfully used.[3,10] Moreover, the cobalt(II/III)-based redox electrolyte is also attracting researchers' interest.[3,11] Recently, the all-solid-state perovskite structure consisting of $CsSnI_{2.95}F_{0.05}$ doped with SnF_2 as the hole conducting material was implemented.[12] For the part of semiconductor, the anatase TiO_2 has been generally

Received: April 6, 2016
Published: June 10, 2016

DOI: 10.1021/jacs.6b03524
J. Am. Chem. Soc. 2016, 138, 8165−8174

studied as the photoanode both in the experimental[1,5−7,11] and theoretical works.[13−15] The conversion efficiency of DSCs has been stuck at around 11% for 10 years[16] after rapidly growing to 10.8% in the early stages of development. Until recently, the record efficiency reached 12% utilizing a combination of zinc-porphyrin dye, TiO_2, and cobalt(II/III)-based redox[17] and then 13% via molecularly engineering the porphyrin dye.[18]

Nevertheless, some fundamental issues in DSCs remain unsolved, which prevents further improvement of its efficiency to compete with conventional silicon solar cells. One issue is the detailed atomistic mechanism of ET from the dye molecule to the photoanode semiconductor. Because the ET rate in DSCs solar cell is a major element of the overall efficiency of the cells,[19] a great effort has been made to find alternate oxides to replace TiO_2 in order to improve the photoelectron extraction efficiency.[20] For instance, ZnO has a similar band gap ($E_g \sim 3.4$ eV) and electron affinity ($E_A = 4.7$ eV) as anatase TiO_2 ($E_g \sim 3.2$ eV, $E_A = 5.1$ eV),[20−24] but ZnO possesses a much higher electron mobility (200 $cm^2/(V{\cdot}s)$) than that of TiO_2 (1 $cm^2/(V{\cdot}s)$).[25,26] As a consequence, the replacement of TiO_2 by ZnO is expected to enhance the electron extraction rate and thus increase the overall efficiency of DSCs. However, after examining various ZnO phases including thin film, nanowire, nanosheet, nanotube as well as TiO_2/ZnO core/shell structures,[27,28] the highest achieved efficiency of ZnO-based DSCs reported in the literature is only 7.5%,[29] which is 42% lower than that of TiO_2-based DSCs.[18] Recently, a time-resolved spectroscopy experiment demonstrated that the lower efficiency of ZnO-based DSCs is mainly due to the slower ET process from the dye molecule to the ZnO compared with TiO_2-based DSCs.[30] In that experiment, the estimated ET occurs in a few hundreds of picoseconds, which is 3−4 times slower than that from the dye to the TiO_2.[30] Anderson et al. found that the ET process contains both fast and slow components[31] and the overall ET time for TiO_2 is in tens of picoseconds, 7−16 times faster than that for ZnO (hundreds of picoseconds). Although the measured ET rates by these two experiments have differences in a few times, both of them clearly illustrated that the electron injection/extraction time for ZnO is about 10 times longer than that of TiO_2, which is the main reason that the ZnO-based DSCs have the lower performance than TiO_2-based DSCs.

Although the experimental fact became well established, the underlying mechanism of ET from the dye to the semiconductor still remains ambiguous. Several hypotheses have been proposed to explain the unexpected much slower ET in ZnO-based DSCs. Hypothesis A: Zn^{2+}-dye complexes forming on the ZnO surface induce the electron trap states on the surface, while they are absent in TiO_2-based DSCs. These surface electron states are responsible for the slow ET in ZnO-based DSCs since they can suppress the ET process from the dye molecule to the ZnO.[32] Hypothesis B: The electron coupling between the ZnO conduction band states and the dye molecule states is weaker than that of the TiO_2.[31] Hypothesis C: The number of available conduction band states in ZnO is much smaller than that in TiO_2 to accept the electron injected from the dye molecule.[30,33] Hypothesis D: The lower static dielectric constant of ZnO (∼8) compared with that of TiO_2 (∼100) has also been considered as the reason for the slow ET in ZnO-based DSCs.[34] Unfortunately, all these hypotheses are pure speculations rather than based on the solid experimental or theoretical evidence. Why the photoexcited ET in the TiO_2-based DSCs is faster than that in the ZnO-based DSCs remains a major puzzle.

In this work, we systematically investigate the ET process from the dye molecule to anatase TiO_2 and ZnO films, respectively, by performing the first-principles calculations. We have developed a general procedure based on the Marcus theory, which enables us to carry out a detailed atomistic study of ET process in relatively large systems. The procedure includes the correction of density functional theory (DFT) error on eigen-energies, the construction of diabatic states, and the proper treatment of solvent contribution to the reorganization energy. Because the Marcus theory of ET is reliable based on a corrected Hamiltonian obtained initially from the DFT calculation, the predicted ET rates agree well with the experimental values. We find that the underlying mechanism responsible for the much faster ET in TiO_2-based DSC is due to the denser intermediate states between the TiO_2 CBM and the lowest unoccupied molecular orbital (LUMO) state of the dye molecule. Whereas, the coupling constants in both TiO_2- and ZnO-based DSCs are rather similar. We then propose alternative pathways to improve the efficiency of DSCs via enhancing the ET rate.

METHODS

Model of the Dye Molecule/Semiconductor System. In DSCs, the zinc-porphyrin (YD2-o-C8) molecules are usually used as the sensitizing dye[17] and are anchored to particles of wide-bandgap semiconductor such as TiO_2 or ZnO. The TiO_2 particles have been observed to own (101) facts[2,35] and are about 10 nm in diameter.[27] The density of the dye molecules on the TiO_2 facts is estimated to be about 1 dye molecule per square nanometer.[36] To study the ET from the zinc-porphyrin (YD2-o-C8) dye molecules to TiO_2 particles in real DSCs, we construct a model of one dye molecule adsorbed on a TiO_2 (101) slab, placed in a periodic supercell as shown in Figure 1a. In DSCs, carboxylic acid groups (−COOH) of the YD2-o-C8 dye molecule are experimentally found to be the linker to the TiO_2 surface.[4,37] Vittadini et al. have theoretically revealed that the most stable adsorption configuration of the formic acid on the TiO_2 (101) surface is the "monodentate" mode, which is one of the two O atoms

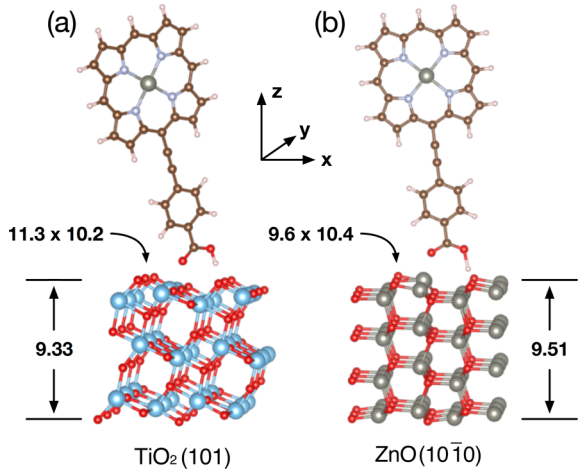

Figure 1. Semiconductor + dye molecule structure used in the calculation. (a) The YD2-o-C8 dye moleucle is attached on the TiO_2 slab. The supercell inside the *xy* plane is 11.3 × 10.2 Å. The TiO_2 film is 9.33 Å thick, containing six Ti layers. (b) ZnO + dye molecule system. The supercell inside the *xy* plane is 9.6 × 10.4 Å. The ZnO film is 9.51 Å thick, with eight Zn layers. The vacuum for both systems is 12 Å.

DOI: 10.1021/jacs.6b03524
J. Am. Chem. Soc. 2016, 138, 8165−8174

and the H atom of the formic acid preferring to bind with 5-fold coordinated Ti atom and 2-fold coordinated O atom of the TiO_2, respectively.[38] Following this absorption mode, we have constructed a model of dye molecule adsorbed on the TiO_2 slab model. The lateral size of the supercell is 11.3 × 10.2 Å, corresponding to a density of one dye molecule per square nanometer as found experimentally in DSCs.[36] The TiO_2 slab consists of six monolayers, corresponding to a thickness of 9.33 Å. On top of the dye molecule a 12 Å thick vacuum is added in the vertical direction of the supercell in order to avoid the interaction with its images. More details can be found in ref 38 and Figure S1. The calculation of the YD2-o-C8 dye molecule has shown that the LUMO state, which is the only dye molecule state involved in our study, is mainly localized in the light-sensitized part. The side wings of YD2-o-C8 barely contribute to the LUMO.[8] Therefore, we could safely remove the side wings without influencing on the calculated results and build a simplified model to reduce the computational cost. In order to minimize the strain energy, we relax the atom positions to the ground state by performing the DFT calculation, while keeping the atom positions of inner layers of the TiO_2 slab fixed to the bulk positions to mimic a realistic thick slab. Figure 1a shows the relaxed geometric structure of the TiO_2 + dye molecule system, in which the obtained bonding structure (such as bond lengths and bond angles) near the interface is in excellent agreement with that predicted by Vittadini et al.[38]

Following the same procedure, we have also constructed the model of YD2-o-C8 adsorbed on the ZnO $(10\bar{1}0)$ surface. In order to reduce the difference arising from the quantum confinement in the slab, the ZnO slab is set to contain eight monolayers and is 9.51 Å thick, which is as close as possible to the TiO_2 slab. The lateral size of the supercell is 9.6 × 10.4 Å. Similar to the TiO_2 + dye system, here the dye molecule is attached to the ZnO surface through the −COOH group. Persson and Ojamäe have theoretically found that the so-called "unidentate structure" is the most stable adsorption mode.[39] In this case, one of two O atoms of the −COOH group is bound directly to the Zn dangling bond, and a hydrogen bond is formed between the H atom of the −COOH group and the O atom of ZnO, as shown in Figure 1b. The atom positions are then relaxed to the ground state, but again keeping the atom positions of inner layers of the ZnO slab fixed to that of the bulk ZnO crystal. For more details see ref 39 and Figure S1.

Marcus Theory Formula. When the dye molecule absorbs an incident photon, an electron is excited from an occupied molecular orbital to an unoccupied molecular orbital, leaving a hole behind (generating an electron−hole pair). The photoexcited electron and hole will then relax to the LUMO and highest occupied molecular orbital (HOMO) state inside the dye molecule, respectively, on a time scale of 1 fs. After that, the electron transfers from the dye LUMO state to one of the conduction band states of the attached TiO_2 or ZnO particle and subsequently relaxes to the CBM in an ultrafast phonon-assisted process. Since the molecule is immersed in the electrolyte filled with redox, the hole usually shuffles out the dye molecule before the electron transfers into the semiconductor. But we should point out that the main conclusion presented in our work will not change even if the hole remains in the molecule when the electron is transferring. Such ET process can be described properly by the Marcus theory,[40] which has been demonstrated to describe correctly the ET process between molecule and quantum dot[41] or between the connected quantum dots.[42] Regarding the Marcus theory, the ET rate from the dye LUMO state to the i-th conduction band state of the TiO_2 or ZnO is

$$\nu_i = \frac{2\pi}{\hbar}|V_c^i|^2\left(\frac{1}{4\pi\lambda k_B T}\right)^{1/2}\exp\left\{-\frac{(\Delta G+\lambda)^2}{4\lambda k_B T}\right\} \quad (1)$$

where V_c^i is the coupling constant between the dye LUMO and i-th conduction band of the TiO_2 or ZnO, $\Delta G = G_f - G_i$ is the Gibbs free energy difference corresponding to the system before (G_i) and after (G_f) ET, k_B is the Boltzmann constant, T the temperature, and λ the reorganization energy, which is described in detail in the following section. The ET process is shown in Figure 2. The summation over all possible transfer channels gives rise to the overall ET rate: $\nu = \sum_i \nu_i$.

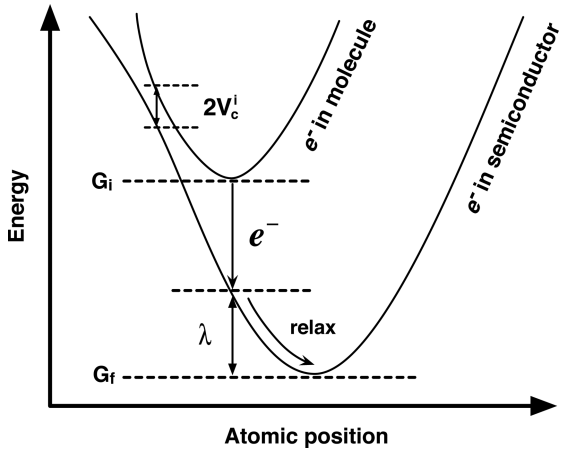

Figure 2. Marcus theory energy potential diagram. The horizontal axis represents all atomic positions. G_i and G_f is the total Gibbs free energy when the electron resides in the dye molecule and semiconductor slab, respectively, λ is the reorganization energy, and V_c^i is the coupling constant between the LUMO and i-th conduction band.

For the initial system i (before ET), an extra electron occupies the LUMO of the dye molecule in addition to all valence band states (including the HOMO) are fully occupied with N electrons, and the atomic positions of the whole system are relaxed to the lowest energy configuration. For the final state f (after ET), this extra electron occupies the i-th conduction band state of the TiO_2 or ZnO. Thus, the Gibbs free energies can be written as

$$G_i = E_N(R_N) + E_{LUMO} - \lambda_{dye} \quad (2)$$

$$G_f = E_N(R_N) + E_i - \lambda_{SC} \quad (3)$$

where $E_N(R_N)$ is the total energy of the charge neutral system (N electrons) with atoms staying at R_N. E_{LUMO} is the quasi-particle energy of the molecular LUMO and E_i is the quasi-particle eigen energy of i-th conduction band of the semiconductor. λ_{dye} and λ_{SC} (SC = TiO_2 or ZnO) are the reorganization energies accounting for the energy addition of the system due to the extra electron in the dye molecule and semiconductor, respectively.

From the above text, we learn that once we obtain all parameters required by the Marcus theory, the calculation of the ET rate becomes straightforward. Therefore, studying the ET turns to calculate the related parameters, i.e., V_c^i, $E_N(R_N)$, E_{LUMO}, λ, λ_{dye}, λ_{SC} of dye + semiconductor systems. In this work, we carry out the first-principles calculations to obtain these parameters in a procedure described below to study the ET process based on the Marcus theory.

DFT Electronic Structure Calculations. The first step of the procedure is to obtain the single particle's energy levels (ϵ_i) and wave functions (ϕ_i) of the dye molecule + semiconductor models by solving the corresponding Schrödinger equations:

$$\left[-\frac{1}{2}\nabla^2 + V_{es}(\mathbf{r}) + V_{ex}(\mathbf{r}) + V_{nl}\right]\phi_i = \epsilon_i\phi_i \quad (4)$$

where $V_{es}(\mathbf{r})$ is the electrostatic potential determined by the total charge density, $V_{ex}(\mathbf{r})$ is the local density approximation (LDA) exchange−correlation energy, and V_{nl} is the nonlocal part of atomic pseudopotentials. We perform the DFT calculation using the plane wave nonlocal pseudopotential code called PEtot and its GPU version PWmat code, which has been proved to be accurate and efficient to calculate large (up to a few thousand atoms) semiconductor systems.[41,43] From our realistic structure calculation, we see that within the energy window we are concerned with, there are no trap states strongly localized at the surface of the semiconductor. The

DOI: 10.1021/jacs.6b03524
J. Am. Chem. Soc. 2016, 138, 8165−8174

absence of surface states, at least in a nicely synthesized system, rules out the (hypothesized) effect of the surface trap states on the ET process.

DFT Energy Level Corrections. The second step of the procedure is to correct the DFT predicted eigen energies. It is well-known that the DFT usually underestimates significantly the band gap of the semiconductors and does not yield correct quasi-particle eigen energies. However, getting the correct eigen energies and band alignment is quite critical for studying the ET. Different approaches have been used to correct the DFT eigen energies. One approach is the GW quasi-particle approximation, which has been used, e.g., to correct the energy alignment in CdSe-quantum rod/ferrocene molecule heterojunction.[41] The another one is the hybrid functional approach. However, both approaches are too expensive to compute the whole dye/semiconductor systems. More importantly, the GW band gap of ZnO is still in debate.[44] The hybrid functional approach underestimates remarkably the ZnO band gap, e.g., 2.49 eV predicted by HSE06 vs 3.44 eV measured by the experiment,[45] although it reproduces reasonably experimental value for TiO_2. We are able to adjust the parameters of the hybrid functional to reproduce well the band gap for ZnO, but the same parameters will overestimate the band gap of TiO_2. Besides, adjusting parameters in that way can make the result "empirical" in nature.

Here, we use a newly developed approach[46] which is more efficient and, more importantly, suitable for both molecules and semiconductors. For the molecule, we apply the ΔSCF method instead of GW corrections to provide accurate quasi-particle energies.[46−48] We correct the bulk CBM positions of the TiO_2 and ZnO based on the LDA potential,[41] and a new Wannier Koopman's theory is used.[46] Such method can yield accurate semiconductor band gap as well as band alignment.

In our model, both the TiO_2 and ZnO slabs have finite thickness, so we have to consider the quantum confinement effect of the slab on the band gap. When the dye molecule is attached to the semiconductor surface, there is another effect due to the long-range polarization of the semiconductor surface.[49] Such polarization potential P is also included to correct the LUMO energy. All these corrections are well established in our previous studies.[46] See the Supporting Information for more details.

The energy levels of the semiconductor + dye molecule system before and after ΔSCF + P correction on DFT are shown in Figure 3. The TiO_2 CBM is shifted upward by ΔE_{CBM} = 0.16 eV and the VBM downward by ΔE_{VBM} = −0.40 eV, yielding a band gap of 3.2 eV. The dye LUMO is shifted upward by ΔE_{LUMO} = 0.29 eV. The band offset between LUMO and CBM after the correction is 1.25 eV. For ZnO + dye system, the ZnO CBM is shifted upward by ΔE_{CBM} = 0.49 eV and the VBM downward by ΔE_{VBM} = −2.02 eV. Thus, the band gap is 3.4 eV. The dye LUMO is shifted upward by ΔE_{LUMO} = 0.31 eV. The band offset between LUMO and CBM after the correction is 1.14 eV, which is only 0.11 eV smaller than that of TiO_2 + dye system. The predicted band gaps of TiO_2 and ZnO are in good agreement with the experimental data. We see that the band alignment between the TiO_2 and ZnO dye molecule systems are rather similar.

Modifications of DFT Wave Functions. The third step of the procedure is to modify the DFT predicted wave functions since their corresponding eigen energies are changed. The coupling constants V_c^i in the Marcus theory rely on the wave functions of the initial and final state of the ET reaction. However, after the correction of the DFT eigen energies, the eigen wave functions might be completely changed, e.g., the coupling and hybridization of the wave functions between the dye molecule states and the semiconductor states. Thus, how to yield the correct wave functions for the corrected eigen values is another critical issue for the first-principles calculation of nanoscale ET. One can consider the change of eigen energies as a modification of the DFT Hamiltonian. To represent this change at the subspace of the relevant eigen states, we decompose a relevant DFT eigen state ϕ_i into two parts:

$$|\phi_i\rangle = |\phi_i\rangle\cdot m(\mathbf{r}) + |\phi_i\rangle\cdot[1 - m(\mathbf{r})] = |\phi_{i,1}\rangle + |\phi_{i,2}\rangle \quad (5)$$

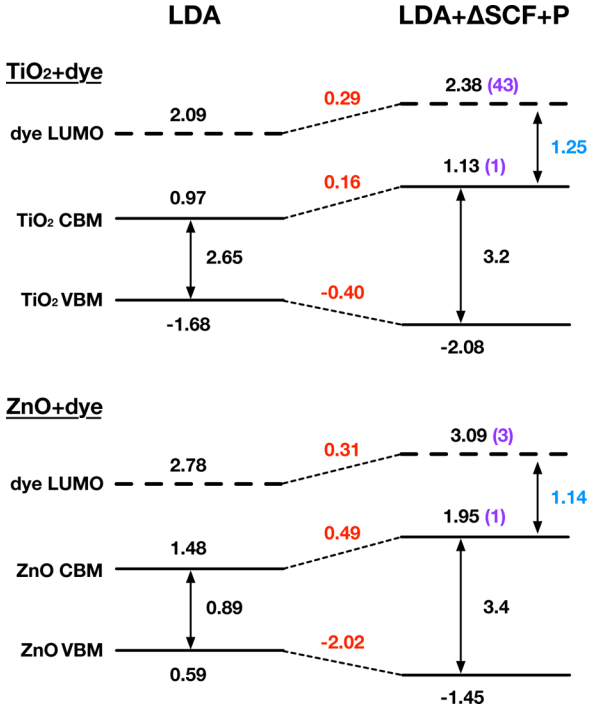

Figure 3. Single particle energy levels predicted by DFT and corrected by adding the ΔSCF + P effect. The purple numbers in the parentheses indicate the band index. All energy values are in eV.

where $|\phi_{i,1}\rangle$ and $|\phi_{i,2}\rangle$ are two parts of the wave function located inside the dye molecule and semiconductor, respectively, and $m(\mathbf{r})$ is a mask function defined as

$$m(\mathbf{r}) = \begin{cases} 1, & \text{if } \mathbf{r} \in \text{dye molecule} \\ 0, & \text{if } \mathbf{r} \in \text{SC} \end{cases} \quad (6)$$

As a consequence, the new Hamiltonian H within the subspace of $\{\phi_i\}$ after the correction of the eigen energy levels is written as

$$H = \sum_i \sum_{a,b=1,2} (\epsilon_i + \Delta_{i,ab})|\phi_{i,a}\rangle\langle\phi_{i,b}| \quad (7)$$

where $\Delta_{i,ab}$ is

$$\Delta_{i,ab} = \begin{cases} \Delta E_{LUMO}, & a = b = 1 \\ \Delta E_{CBM}^{SC}, & a = b = 2 \\ (\Delta E_{CBM}^{SC} + \Delta E_{LUMO})/2, & a \neq b \end{cases} \quad (8)$$

where ΔE_{LUMO} and ΔE_{CBM}^{SC} are the corrections to the DFT eigen energies. Note that if $\Delta_{i,ab}$ = 0, the above Hamiltonian H is the original DFT Hamiltonian within the $\{\phi_i\}$ subspace. We shift all the remaining conduction band states of the semiconductor in energy by the same amount of the energy as the correction to the CBM. The new eigen wave functions ψ_i can be expanded as a linear combination of ϕ_j:

$$\psi_i = \sum_j U_{ij}\phi_j \quad (9)$$

The corrected energy levels (E_i) and wave functions (ψ_i) are obtained by diagonalizing the matrix $\langle\phi_i|H|\phi_j\rangle$, which can be evaluated from eqs 7 and 8. Note, we use $\{\phi_i\}$ instead of $\{\phi_{i,a}\}$ as the basis set, because $\{\phi_{i,a}\}$ is not orthogonal. Moreover, eq 7 merely mixes different ϕ_i.

The Coupling Constants. The fourth step of the procedure is to calculate the coupling constants based on the corrected DFT eigen energies and wave functions. In the DSCs, the photogenerated ETs from the dye molecule LUMO to the SC conduction band states. V_c^i, in the Marcus theory formula eq 1, is thus the coupling constants between these diabatic states (instead of the single particle eigen states,

DOI: 10.1021/jacs.6b03524
J. Am. Chem. Soc. 2016, 138, 8165−8174

see Figure 2).[50,51] There are different ways to calculate V_c^i. A reliable way is to construct the wave functions localized inside the SC and dye molecule, respectively, to represent these diabatic states. In doing so, we first express the wave function localized inside the dye molecule as a linear combination of ψ_i:

$$\psi_L = \sum_i C_i \psi_i \text{ and } \sum_i C_i^2 = 1 \tag{10}$$

We then ensure ψ_L to be localized in the dye molecule region by maximizing the integration of $F = \int |\psi_L|^2 m(\mathbf{r}) d^3r$ under the conditions of eq 10. Using Lagrange multipliers, we are able to find the maximum value of F. Specifically, we write the Lagrange function as $L = F - \kappa(\sum_i C_i^2 - 1)$, where κ is the Lagrange multiplier, and the maximum solution of $F(\{C_i\})$ is obtained by solving the equations $\frac{\partial L}{\partial C_i} = 0$. Once we get $\{C_i\}$ and ψ_L, the wave functions of the diabatic states localized inside the SC (which is orthogonal to ψ_L) are obtained as

$$\psi_i' = \frac{1}{\sqrt{1 - C_i^2}}(\psi_i - C_i \psi_L) \tag{11}$$

Finally, the coupling constant V_c^i between the LUMO state ψ_L and the i-th conduction band state ψ_i' is calculated as

$$V_c^i = \langle \psi_i' | H | \psi_L \rangle = \frac{C_i}{\sqrt{1 - C_i^2}}(E_i - \sum_k C_k^2 E_k) \tag{12}$$

The Reorganization Energies. The final step of the procedure is to obtain the reorganization energies of dye molecule (λ_{dye}) and SC (λ_{SC}), which are responsible for the charging induced structure relaxation. The reorganization energies have two parts: one is due to the atomic position relaxation inside the molecule or semiconductor, and the other one is due to the atomic relaxation of the surrounding solvent molecules:

$$\lambda_X = \lambda_X^{atom} + \lambda_X^{sol} \text{ (with X = dye or SC)} \tag{13}$$

For the semiconductor, the TiO_2 and ZnO slab is large enough so that $\lambda_{SC}^{atom} = 0$. We apply the traditional analytical solvent model to obtain the solvent part λ_X^{sol},[52] where it inquires the effective radius of the system. In the experiment of real DSCs, TiO_2 or ZnO conductor is usually formed as a nanoparticle with a 10 nm diameter.[27] So we can write this part as

$$\lambda_{SC}^{sol} = \frac{1}{2}\left(\frac{1}{\varepsilon_\infty^{sol}} - \frac{1}{\varepsilon_0^{sol}}\right)\frac{1}{R_{SC}} \tag{14}$$

where the nanoparticle size is R_{SC} = 10 nm and ε_0^{sol} and ε_∞^{sol} are the static and optical dielectric constant of the solvent, respectively. In this work, we use acetonitrile as the solvent, where ε_0^{sol} = 38.8 and ε_∞^{sol} = 1.8. As a consequence, λ_{SC}^{sol} = 26 meV. Thus, the overall reorganization energy of TiO_2 or ZnO conductor is λ_{SC} = 26 meV.

For the dye molecule, λ_{dye}^{atom} can be obtained by the DFT calculation of an isolated dye molecule. We first relax the atom positions of the neutral molecule (with N electrons) to obtain the corresponding atom positions R_N. Then we add an extra electron (N + 1 electrons) to the LUMO and calculate the total energy $E_{N+1}(R_N)$ by fixing the atomic positions to R_N. After that, we relax the atom positions of the negative charged molecule to R_{N+1} and obtain the corresponding total energy $E_{N+1}(R_{N+1})$. We are ready to calcualte $\lambda_{dye}^{atom} = E_{N+1}(R_N) - E_{N+1}(R_{N+1})$, which is λ_{dye}^{atom} = 61 meV for the chosen dye. λ_{dye}^{sol} is calculated using numerical method based on the density-based continuum solvent model, which is recently developed to include the solvent effects in density functional calculations,[53,54] because the dye molecule is too small to use analytical formulas like eq 14. The advantage of this method is that it involves few empirical parameters and reproduces many experimental solvent screening effects. In contrast to the simple analytical solvent model,[52] it can treat the charge with arbitrary shapes, not only the spherical ones. This feature is important for our problem since the dye molecule LUMO state has a flat shape, which cannot be described simply by an analytic formula. For more details, see the Supporting Information. Based on above method, we predict λ_{dye}^{sol} = 406 meV. The overall reorganization energy of the dye molecule is thus obtained as $\lambda_{dye} = \lambda_{dye}^{atom} + \lambda_{dye}^{sol}$ = 467 meV.

The reorganization energy λ that appears in eq 1 accounts for the ET from the dye molecule to the SC and approxiamtes as[52]

$$\lambda = \lambda_{SC} + \lambda_{dye} - \left(\frac{1}{\varepsilon_\infty^{sol}} - \frac{1}{\varepsilon_0^{sol}}\right)\frac{1}{D} \tag{15}$$

where D is the distance between the center of mass of the dye molecule and the SC nanoparticle center. In this work, D = 112 Å because the radius of TiO_2 or ZnO nanoparticle is about 10 nm[27] and the size of the dye molecule is about 12 Å. So λ = 425 meV.

Once we have the reorganization energies, the exponent term in the Marcus theory formula (see eq 1) is obtained as

$$\begin{aligned} \Delta G + \lambda &= E_i - E_{LUMO} + \lambda_{dye} - \lambda_{SC} + \lambda \\ &= E_i - E_{LUMO} + \lambda_{all} \end{aligned} \tag{16}$$

where $\lambda_{all} = 2\lambda_{dye} - \left(\frac{1}{\varepsilon_\infty^{sol}} - \frac{1}{\varepsilon_0^{sol}}\right)\frac{1}{D}$ = 866 meV. Note that λ_{all} depends only on λ_{dye}. The contribution of the semiconductor on λ comes only from the band offsets between the CBM and LUMO. All predicted parameters required by the Marcus theory formula are listed in Table 1.

Table 1. Parameters Used in the Calculation of the Marcus theory

R_{SC}	10 nm	λ_{SC}	26 meV
D	112 Å	λ_{dye}	467 meV
ε_∞^{sol}	1.8	λ	425 meV
ε_0^{sol}	38.8	λ_{all}	866 meV
T	300 K		

In summary, we have developed a procedure to perform first-principles calculations of ET rates based on the Marcus theory of ET for DSCs. Once we constructe the model of dye molecule adsorbed on the semiconductor substrates, we first calculate the single-particle eigen energies and wave functions of the dye + semiconductor system using the DFT functionals. Then, we correct the well-known DFT errors on bandgap and band alignment using our recently developed ΔSCF scheme.[46] Then, the diabatic states are constructed by the linear combination of corrected DFT wave functions to calculate the coupling constants. Finally, we calculate the reorganization energies of dye molecule and SC. Once we obtain all these parameters required by the Marcus theory, the calculation of the ET rate becomes straightforward.

RESULTS

Figure 4 shows the predicted ET rates of both TiO_2- and ZnO-based DSC systems as functions of the band offsets between the dye LUMO and CBM state ($E_{LUMO} - E_{CBM}$). The open circles are the results calculated by DFT. The solid circles are the results when we artificially change the band offsets. We see that, in TiO_2/dye system, $E_{LUMO} - E_{CBM}$ = 1.25 eV; the ET rate $\nu = 1.15 \times 10^9$ s^{-1}, which corresponds to a ET time of 1 ns. This is the theoretical upper limit of the ET time. In experimental measurements, the ET time is deduced from the photoelectron optical spectra, and other recombination processes such as Auger recombination could also decrease the photoelectron lifetime inside the dye molecules.[55,56] The upper bound of experimentally reported ET times is indeed around 1 ns.[2] For the ZnO/dye model system, the calculated ET rate is about 6.87×10^7 s^{-1}. Therefore, the predicted ratio of ET rates between TiO_2- and ZnO-based DSCs is about 15, within the experimentally observed range of 3−16.[31]

DOI: 10.1021/jacs.6b03524
J. Am. Chem. Soc. 2016, 138, 8165−8174

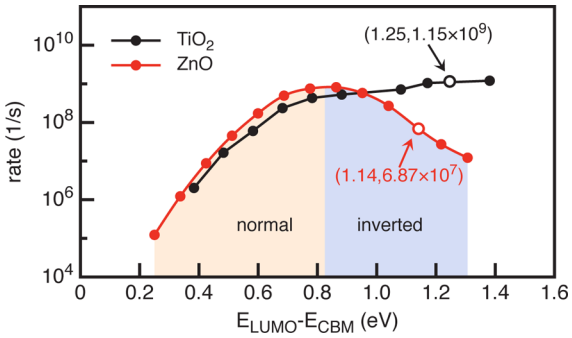

Figure 4. Dependence of the ET rate on the thermodynamic driving force for the ET reaction. The thermodynamic driving force, the Gibbs free energy difference ΔG, here mainly depends on the energy position of the dye LUMO (E_{LUMO}) with respect to the semiconductor CBM. Therefore, ν, here, is inspected as a function of $E_{LUMO} - E_{CBM}$ by artificially varying the E_{LUMO} and fixing the energy position of the CBM. The open circles are the results corresponding to real TiO_2-based or ZnO-based DSCs.

DISCUSSION

Regarding the Marcus theory, four factors determine the overall ET rate ν: (i) wave function coupling constant V_c^i. Hypothesis B argues that the experimentally observed faster ET rate in the TiO_2-based DSCs is due to a larger coupling constant.[31] But in our case, we do not see any significant difference between the TiO_2 and ZnO systems. (ii) Reorganization energy of the dye molecule λ_{dye}, which can affect λ (see method section). Hypothesis D argues that the lower static dielectric constant of ZnO (~8) compared with that of TiO_2 (~100) leads to a smaller free energy of ET reaction and, therefore, leads to a slower ET in ZnO-based DSCs.[34] However, we find the reorganization energies of TiO_2 and ZnO systems are quite similar, which excludes the hypothesis D. (iii) Energy band offset between the dye LUMO and TiO_2 or ZnO CBM. Our first-principles calculation predicts that energy positions of the TiO_2 CBM and ZnO CBM are too close to lead to the observed ET rate difference between TiO_2 and ZnO-based DSCs. Our result is consistent with the experiment, which claims that the band offset is not the main reason for the ET rate difference.[33] (iv) Available ET channels. Based on our first-principles calculation, we demonstrate that the much denser conduction band states of the TiO_2 compared with ZnO provide more available ET channels and thus lead to faster ET in the TiO_2-based DSCs. We, therefore, theoretically prove the validity of the hypothesis C.[30,33]

Besides the above four physical parameters, hypothesis A argues a different mechanism causing the observed low ET rate in ZnO-based DSCs. It assumes the surface electron trap states, arising from Zn^{2+}-dye complexes formed on the ZnO surface, will suppress the ET process and therefore lead to the low ET rate in ZnO-based DSCs.[32] These surface electron states are absent in the TiO_2-based DSCs. Without involving the surface states, our predicted ET rates of both TiO_2 and ZnO-based DSCs are already in good agreement with experimental results. We can therefore exclude the hypothesis A.[32]

A plot of ν as a function of ΔG is usually utilized in the literature to examine the dependence of the ET rate on the thermodynamic driving force for the ET reaction.[57] In the current work, ΔG mainly depends on the energy position of the LUMO state (E_{LUMO}) relative to the semiconductor CBM. Therefore, ν, is inspected as a function of $E_{LUMO} - E_{CBM}$, shown in Figure 4, by artificially varying the E_{LUMO} and fixing the energy position of the CBM. In the experiments, this varying could be realized by adding different side groups on the dye molecule[3] or modifying the concentration of the dye and lithium cations in the electrolyte.[58] For the ZnO system, this dependence yields a typical inverted bell-shaped curve of Marcus theory with a maximum rate constant when $E_{LUMO} - E_{CBM} = \lambda_{all}$ (λ_{all} depends only on the reorganization energy of the system and will be discussed in the Methods section).

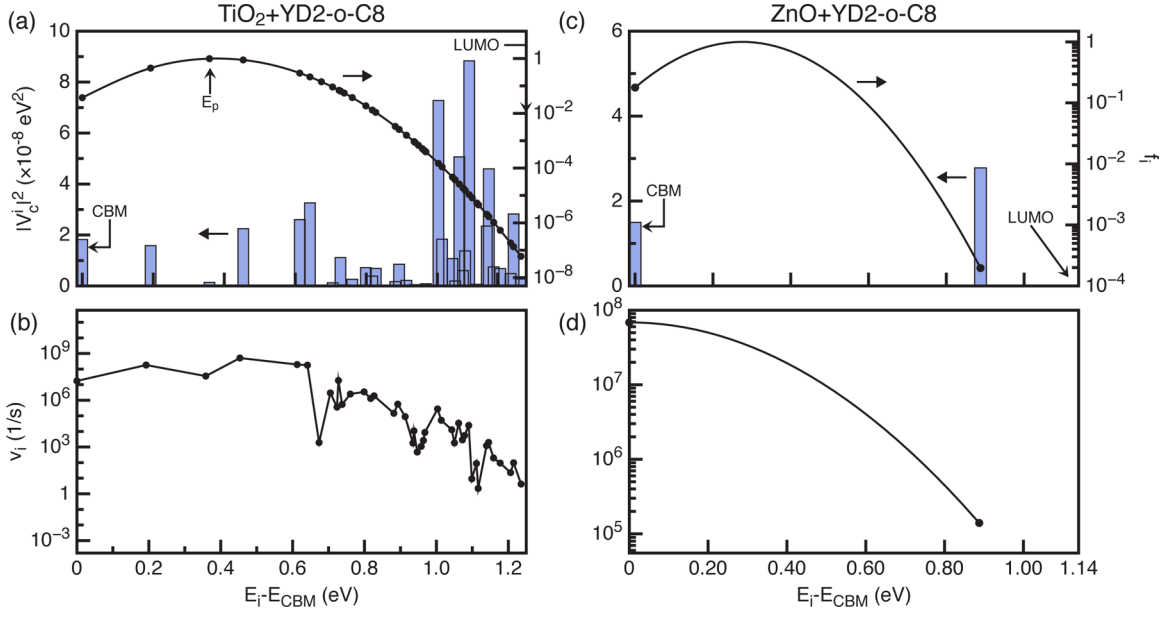

Figure 5. Decomposition of the overall ET rate into individual ET channels. (a and c) The predicted wave function coupling constant $|V_c^i|^2$ (blue bars) between the LUMO and i-th conduction band state of semiconductors for both TiO_2 + YD2-o-C8 and ZnO + YD2-o-C8 systems. The exponential part $\exp\{-(\Delta G + \lambda)^2/4\lambda k_B T\}$ in Marcus theory are also given as the black line. (b and d) The decomposed ET rate ν_i from the LUMO to i-th conduction band state for TiO_2 + YD2-o-C8 and ZnO + YD2-o-C8 systems, respectively.

DOI: 10.1021/jacs.6b03524
J. Am. Chem. Soc. 2016, 138, 8165−8174

When $E_{LUMO} - E_{CBM} < \lambda_{all}$, the reaction is in the so-called normal Marcus region, which is consistent with the intuitively expected behavior of the transfer rate to vary with the thermodynamic driving force. In this region, as $E_{LUMO} - E_{CBM}$ becomes larger, the activation barrier decreases, and the ET rate increases by several orders of magnitude. Eventually, when $\lambda_{all} = E_{LUMO} - E_{CBM}$, there is no vibrational barrier to ET and ν reaches a maximum (often the celling for the ET rate constant reaches the diffusion-controlled limit). $E_{LUMO} - E_{CBM} > \lambda_{all}$, the reaction is in the inverted Marcus region. In this region, the rate of ET decreases even when $E_{LUMO} - E_{CBM}$ becomes larger. It is surprising to see that the ZnO/dye system (the red open circle in Figure 4) is in the inverted Marcus region. The systems in the inverted region are vary rare. It takes a few decades to find the first example of ET reaction to support the Marcus theory after Marcus postulated the existence of the inverted region.[59]

In the case of TiO_2-based system, we, however, find an unexpected dependence of ν on $E_{LUMO} - E_{CBM}$, as shown in Figure 4. In this dependence, there is no transition between the normal and inverted region. The system is always in the normal region within the energy range we examined. Nevertheless, our predicted ν is well supported by the experimental evidence. For instance, Koops et al. reported that a 280 meV shift in CBM state could result in an 8-fold increase of ET rate.[58] In our calculation, the 280 meV energy shift correspond to the 4-fold enhancement. Moreover, the predicted ET rate corresponds to theoretical ET time of 1 ns, which is the upper bound of experimental values.[2]

It is surprising that the ET process of the two systems are strikingly distinct in terms of $E_{LUMO} - E_{CBM}$ since they have the similar energy band positions. Figure 3 shows that there is only one intermediate state lying between the CBM and LUMO in the ZnO system. However, in the TiO_2 system, there are 41 intermediate states. These intermediate states all belong to the semiconductor since they locate on the semiconductor side. Although the number of such intermediate states depends on the size of the TiO_2 and ZnO slabs used in our calculations, the density of state (DOS) near the CBM of TiO_2 is certainly much higher than that of ZnO, as exhibited in Figure 7a. This finding makes sense because the conduction band effective mass of TiO_2 ($\sim 10m_0$, where m_0 is the free electron mass)[60] is about 43 times larger than that of ZnO ($\sim 0.23m_0$).[61]

These intermediate states provide additional ET channels from the LUMO of the dye molecule to the CBM of the semiconductor. In other words, the electron could transfer from the LUMO to these semiconductor intermediate states and then further relax to the CBM. The ET rate in DSCs, as shown in Figure 4, is thus the summation over all possible ET channels. Here, we analyze the contributions of individual conduction band state to the overall ET rate. Figure 5 shows the ET rates and coupling constants of individual transfer channels for both TiO_2 and ZnO systems. We find that the coupling constants between the CBM and LUMO in ZnO system are almost the same as that in TiO_2 system. We, therefore, exclude the hypothesis B, which is based on the argument of different coupling constants, to explain the experimentally observed 15-fold faster of the ET rate in TO_2-based DSCs than that in ZnO-based DSCs.

The energy-dependent exponential factor $f_i = \exp\{-(E_i - E_{LUMO} + \lambda_{all})^2/4\lambda k_B T\}$ in the Marcus theory (see eqs 1 and 16) regulates, beyond the coupling constant, the contributions of individual channels to overall ET and is shown as the black lines in Figure 5a,c. This term tells that the largest f_i is at about $E_p \approx 0.3$ eV above the CBM, corresponding to the transition point. The ET channel with its energy lower than this transition point is in the normal Marcus region and higher than this point is in the inverted region. The individual channel ET rate ν_i is proportional to $|V_{cl}^i|^2 \times f_i$. The contribution of a certain ET channel to the overall ET rate ν is becoming negligible when its energy is away from the transition point, owing to f_i decreasing so dramatically. In the TiO_2 system, if the lowest six conduction band states are close to the transition point possessing large f_i, they contribute remarkably to the overall ET rate (see Figure 5b). Specifically, the second conduction band state above the CBM (CBM + 2) has a relatively small coupling constant, but its contribution to the overall ET rate is similar as the CBM because it is at the transition point and has the largest f_i. Whereas, in the ZnO system, the only available ET channel is the CBM. The contribution even from the CBM + 1 is almost negligible because its energy is far away from the transition point, as shown in Figure 5c. We now understand that the much larger DOS around the Marcus transition point is responsible for the faster ET rate observed experimentally in the TiO_2-based DSCs than that in ZnO-based ones.

In ZnO-based DSCs, the predicted band offset between the CBM and LUMO is so large (1.14 eV) that the CBM ET channel is in the inverted Marcus region. The first excited state CBM + 1 is so close to the LUMO that it is negligible to overall ET rate, although it is in the normal Marcus region. Consequently, the predicted overall ET in ZnO-based DSCs is in the inverted Marcus region. In TiO_2-based DSCs, although the CBM as well as CBM + 1 ET channels are in the inverted Marcus region, there are four important ET channels (CBM + 2, ..., CBM + 5) in the normal region. Therefore, the predicted overall ET in TiO_2-based DSCs is in the normal region. We could conclude that the mystery responsible for the striking distinct of ν versus $E_{LUMO} - E_{CBM}$ between ZnO and TiO_2 systems is much denser intermediate states between the CBM and LUMO in TiO_2-based DSCs than that in ZnO-based ones.

The reorganization energy λ_{dye} also plays an important role in the overall transition rate. We have investigated the dependence of the ET rate ν on λ_{dye}. The results are shown in Figure 6. For TiO_2, as λ_{dye} increases, ν decreases monotonously. For ZnO-based cells, as λ_{dye} increases, ν first increases and then decreases. We find that ν will reach the maximum value at about $\lambda_{dye} = 604$ meV. When $\lambda_{dye} < 604$ meV, the ET in ZnO-based cells is in the inverted Marcus region (blue part in Figure

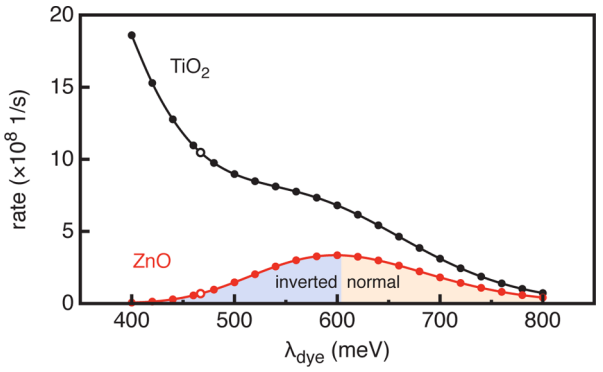

Figure 6. Overall ET rate as a function of artificially varied λ_{dye}. The open circles are the corresponding results for real TiO_2 and ZnO-based DSCs, respectively.

DOI: 10.1021/jacs.6b03524
J. Am. Chem. Soc. 2016, 138, 8165−8174

6). When λ_{dye} is larger, the ET reaches to the normal Marcus region (yellow part in Figure 6) and begins to decrease. For TiO_2-based cells, the ET is in the normal region and transition between normal and inverted regions is not so obvious since there are many states contributing to the transition rate. The change of λ_{dye} can be obtained by changing the dielectric property of the solvent molecules.

In the above discussion, we use a slab with the finite thickness to model semiconductors (see the Methods section), and only the Γ point is considered. This approximation leads to a finite number of conduction band states. However, in the real DSCs, semiconductor nanoparticles are usually about 10 nm in diameter, and their electronic properties are closer to their bulk parents. We learn that the number of intermediate states is important for ET process, so we have to consider the bulk TiO_2 or bulk ZnO in DSCs because they have continued energy bands instead of discrete energy levels. The corresponding formula of the ET rate for bulk semiconductor is rewritten as

$$\nu = \frac{2\pi}{\hbar}|V_c^{bulk}|^2\left(\frac{1}{4\pi\lambda k_B T}\right)^{1/2} \int_{CBM}^{\infty} \exp\left\{-\frac{(E - E_{LUMO} + \lambda_{all})^2}{4\lambda k_B T}\right\} n(E)\mathrm{d}E \quad (17)$$

where $|V_c^{bulk}|^2 = (\Omega_{slab}/\Omega_{bulk})|V_c^i|^2$ is the coupling constant for the bulk case and $|V_c^i|^2$ for the slab case (see Figure 5). Ω_{slab} and Ω_{bulk} are the volume of slab supercell and bulk primitive cell, respectively. $n(E)$ is the DOS of the bulk TiO_2 or ZnO calculated by DFT, as shown in Figure 7a. In the derivation of eq 17, we have assumed a universal coupling constant for each semiconductor energy band. As seen from Figure 5, the coupling constants of the CBM between TiO_2 and ZnO are quite similar which will be discussed below, so we adopt a constant of $|V_c^i|^2 = 1.0 \times 10^{-8}$ (eV^2) for both TiO_2 and ZnO slabs. Therefore, $|V_c^{bulk}|^2 = 1.6 \times 10^{-7}$ (eV^2) for the bulk TiO_2 and $|V_c^{bulk}|^2 = 2.1 \times 10^{-7}$ (eV^2) for the bulk ZnO. Figure 7b shows the predicted ET rate for the bulk TiO_2/dye DSC and ZnO/dye DSC. We use the $E_{LUMO} - E_{CBM} = 1.14$ eV for TiO_2 and 1.25 eV for ZnO as in the slab case (open circles in Figure 7b). The solid circles are the results when we artificially change $E_{LUMO} - E_{CBM}$. Because we use the same condition in the calculation for both TiO_2 and ZnO, the ratio of the transfer rate would cancel quite well the uncertainty of the absolute value. Since the calculated $E_{LUMO} - E_{CBM}$ is about 1.14−1.25 eV (the blue range in Figure 7b), the ν_{TiO_2} is about 15 times larger than ν_{ZnO}, which is consistent with the experimental data.[31] Within the $E_{LUMO} - E_{CBM}$ range, this ratio is varying in a range of 10−30.

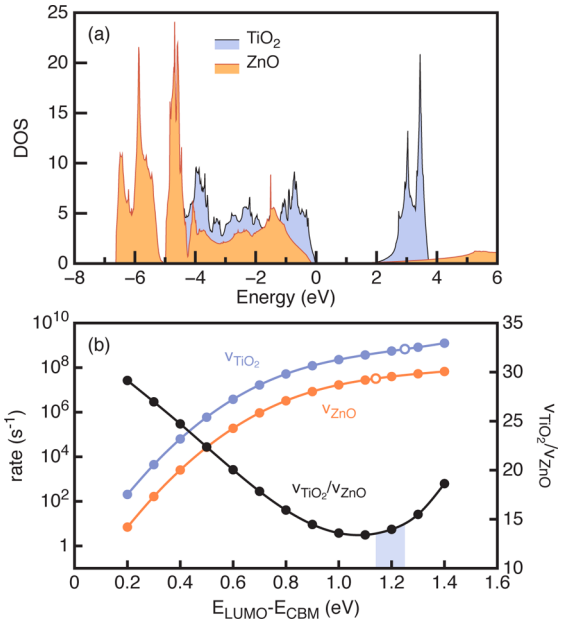

Figure 7. Dependence of the ET rate on the thermodynamic driving force for the ET reaction for bulk semiconductors. (a) DOS of bulk TiO_2 and ZnO. (b) ν_{TiO_2} (blue line), ν_{ZnO} (yellow line), and ν_{TiO_2}/ν_{ZnO} (black line) as functions of $E_{LUMO} - E_{CBM}$ as we artificially change E_{LUMO}.

We note that when the ZnO slab is replaced by the bulk, as shown in Figure 7b, the calculated dependence of ν on $E_{LUMO} - E_{CBM}$ is significantly modified. Like in the TiO_2 slab model, there is also no normal-to-inverted transition. The main difference between a slab and the bulk is a single energy level (slab) versus a band (bulk) with continuum energy dispersion. This change of the ET rate implies the important role of the intermediate states between the LUMO and CBM on the ET rate.

When we replace the slab by the bulk, the energy gap between the CBM and CBM + 1 is now filled in bulk ZnO by more conduction band states. Thus, in a real ZnO-based DSC, more available channels besides the CBM contribute to the overall ET rate. Although the CBM channel is in the inverted Marcus region, after taking into account all available channels, the ZnO-based DSC is actually in the normal Marcus region, as shown in Figure 7b. Our finding may explain why the systems in the inverted region are rare. This is due to most of systems possessing multiple ET or reaction channels. From Figure 7a we see that the conduction band DOS of bulk TiO_2 is about 50 times larger than that of bulk ZnO. As a result, the ET rate in ZnO is much smaller than that in TiO_2 regardless that both systems are in the Marcus normal region.

The high mobility of semiconductors is a highly desired property for photovoltaics including DSCs. However, small effective electron mass in the semiconductors, which is responsible for the high electron mobility, leads to the DOSs for ET channels sparse and is an unfavorable property for DSCs. After revealing that the density of available ET channels is responsible for the fast ET and hence high efficiency of TiO_2-based DSCs, we can propose schemes to improve the efficiency of DSCs. For instance, we could engineer the interface between TiO_2 and dye molecule by, e.g., doping, to increase further the number of available ET channels for enhancing the efficiency of TiO_2-based DSCs. We could also deposit a thin layer of TiO_2 on top of ZnO to provide the required high DOSs to accept photogenerated electrons from dye molecules on the surface and gain the benefit from high mobility of ZnO.

CONCLUSION

We have revealed the origin responsible for the faster ET in the TiO_2-based DSCs than in the ZnO-based DSCs. The calculated electron coupling constants as well as the band alignment between the TiO_2- and ZnO-based DSCs are quite similar. We find that the predominant difference comes from the electron DOSs near the conduction band edge of the photoanode semiconductors. The intermediate states between the dye

DOI: 10.1021/jacs.6b03524
J. Am. Chem. Soc. 2016, 138, 8165−8174

LUMO and semiconductor CBM, particularly, the states energetically close to the CBM, provide additional efficient ET channels. The ZnO owns a much smaller electron effective mass, which is the reason for its much larger electron mobility, but also simultaneously has a much smaller DOSs near the CBM. On the contrary, the TiO_2 owns a larger DOSs, although its mobility is much smaller due to its larger electron effective mass. Therefore, the denser electron states near the CBM provide efficient ET channels and render much faster ET in TiO_2-based DSCs than in ZnO-based DSCs. The 13% recorded efficiency of TiO_2-based DSCs compared to 7% of ZnO-based DSCs indicates that the ET rather than the mobility is the major bottleneck of DSCs. It is impossible for one photoanode semiconductor to possess both higher mobility and larger DOSs near the CBM. According to our conclusion, we could boost the efficiency of DSCs via surface engineering of high mobility photoanode semiconductors, e.g., ZnO, to increase number of the intermediate states between the dye LUMO and CBM at the interface to enhance the ET rate, while also taking advantage of high mobility of photoanode. We have to stress that we should carefully design the surface to avoid the introduction of carrier lifetime killing (recombination) centers.

We also find that the denser ET or reaction channels render the systems to be out of the inverted Marcus region. Our finding may explain why the systems in the inverted region are very rare, taking a few decades to find the first example of ET reaction to support the Marcus theory after Marcus postulated the existence of the inverted region.[59] This is due to most of systems possessing multiple ET or reaction channels.

To study the ET of DSCs, we have developed a systematic procedure to correct the errors in the DFT Hamiltonian. In particular, we have introduced an corrected Hamiltonian based on the DFT eigen energies and wave functions within the subspace of the ET relevant states. This corrected Hamiltonian will remix different states of the substrate and the molecule. Thus, we believe this could be a general procedure applicable for many ET calculations and hope our work would be helpful for the further experiments in the DSCs.

■ ASSOCIATED CONTENT

Supporting Information

The Supporting Information is available free of charge on the ACS Publications website at DOI: 10.1021/jacs.6b03524.

Experimental details and data (PDF)

■ AUTHOR INFORMATION

Corresponding Authors

*jwluo@semi.ac.cn

*lwwang@lbl.gov

Notes

The authors declare no competing financial interest.

■ ACKNOWLEDGMENTS

This work was supported by the National Young 1000 Talents Plan and the National Science Foundation of China (NSFC grant nos. 61474116 and 11374293) (H.W. and J.W.L.) and the U.S. Department of Energy, Director, Office of Science, Office of Basic Energy Sciences, Materials Sciences and Engineering Division, under Contract No. DE-AC02-05CH11231, through the Material Theory program [KC2301] in Lawrence Berkeley National Laboratory (L.W.W.).

■ REFERENCES

(1) O'Regan, B.; Grätzel, M. *Nature* **1991**, *353*, 737.

(2) Hardin, B. E.; Snaith, H. J.; McGehee, M. D. *Nat. Photonics* **2012**, *6*, 162−169.

(3) Hagfeldt, A.; Boschloo, G.; Sun, L.; Kloo, L.; Pettersson, H. *Chem. Rev.* **2010**, *110*, 6595−6663.

(4) Robertson, N. *Angew. Chem., Int. Ed.* **2006**, *45*, 2338−2345.

(5) Wang, P.; Klein, C.; Moser, J.-E.; Humphry-Baker, R.; Cevey-Ha, N.-L.; Charvet, R.; Comte, P.; Zakeeruddin, S. M.; Grätzel, M. *J. Phys. Chem. B* **2004**, *108*, 17553−17559.

(6) Clifford, J. N.; Yahioglu, G.; Milgrom, L. R.; Durrant, J. R. *Chem. Commun.* **2002**, 1260−1261.

(7) Wang, Q.; Campbell, W. M.; Bonfantani, E. E.; Jolley, K. W.; Officer, D. L.; Walsh, P. J.; Gordon, K.; Humphry-Baker, R.; Nazeeruddin, M. K.; Grätzel, M. *J. Phys. Chem. B* **2005**, *109*, 15397−15409.

(8) Han, L.-H.; Zhang, C.-R.; Zhe, J.-W.; Jin, N.-Z.; Shen, Y.-L.; Wang, W.; Gong, J.-J.; Chen, Y.-H.; Liu, Z.-J. *Int. J. Mol. Sci.* **2013**, *14*, 20171.

(9) Shalabi, A. S.; El Mahdy, A. M.; Assem, M. M.; Taha, H. O.; Soliman, K. A. *J. Nanopart. Res.* **2014**, *16*, 2579.

(10) Wang, P.; Zakeeruddin, S. M.; Moser, J.-E.; Nazeeruddin, M. K.; Sekiguchi, T.; Grätzel, M. *Nat. Mater.* **2003**, *2*, 402−407.

(11) Dong, C.; Xiang, W.; Huang, F.; Fu, D.; Huang, W.; Bach, U.; Cheng, Y.-B.; Li, X.; Spiccia, L. *Angew. Chem., Int. Ed.* **2014**, *53*, 6933−6937.

(12) Chung, I.; Lee, B.; He, J.; Chang, R. P. H.; Kanatzidis, M. G. *Nature* **2012**, *485*, 486−489.

(13) Rego, L. G. C.; Batista, V. S. *J. Am. Chem. Soc.* **2003**, *125*, 7989−7997.

(14) Wu, X.; Chen, Z.; Lu, G. Q. M.; Wang, L. *Adv. Funct. Mater.* **2011**, *21*, 4167−4172.

(15) Ma, J.-G.; Zhang, C.-R.; Gong, J.-J.; Yang, B.; Zhang, H.-M.; Wang, W.; Wu, Y.-Z.; Chen, Y.-H.; Chen, H.-S. *J. Chem. Phys.* **2014**, *141*, 234705.

(16) Chiba, Y.; Islam, A.; Watanabe, Y.; Komiya, R.; Koide, N.; Han, L. *Jpn. J. Appl. Phys.* **2006**, *45*, L638−L640.

(17) Yella, A.; Lee, H.-W.; Tsao, H. N.; Yi, C.; Chandiran, A. K.; Nazeeruddin, M.; Diau, E. W.-G.; Yeh, C.-Y.; Zakeeruddin, S. M.; Grätzel, M. *Science* **2011**, *334*, 629−634.

(18) Mathew, S.; Yella, A.; Gao, P.; Humphry-Baker, R.; Curchod, B. F. E.; Ashari-Astani, N.; Tavernelli, I.; Rothlisberger, U.; Nazeeruddin, M. K.; Grätzel, M. *Nat. Chem.* **2014**, *6*, 242−247.

(19) Nazeeruddin, M. K.; Baranoff, E.; Grätzel, M. *Sol. Energy* **2011**, *85*, 1172−1178.

(20) Chandiran, A. K.; Abdi-Jalebi, M.; Nazeeruddin, M. K.; Grätzel, M. *ACS Nano* **2014**, *8*, 2261−2268.

(21) Özgür, Ü; Alivov, Y. I.; Liu, C.; Teke, A.; Reshchikov, M. A.; Doğan, S.; Avrutin, V.; Cho, S.-J.; Morkoç, H. *J. Appl. Phys.* **2005**, *98*, 041301.

(22) Tang, H.; Lévy, F.; Berger, H.; Schmid, P. E. *Phys. Rev. B: Condens. Matter Mater. Phys.* **1995**, *52*, 7771.

(23) Scanlon, D. O.; Dunnill, C. W.; Buckeridge, J.; Shevlin, S. A.; Logsdail, A. J.; Woodley, S. M.; Catlow, C. R. A.; Powell, M. J.; Palgrave, R. G.; Parkin, I. P.; Watson, G. W.; Keal, T. W.; Sherwood, P.; Walsh, A.; Sokol, A. A. *Nat. Mater.* **2013**, *12*, 798−801.

(24) Swank, R. K. *Phys. Rev.* **1967**, *153*, 844.

(25) Look, D. C.; Reynolds, D. C.; Sizelove, J. R.; Jones, R. L.; Litton, C. W.; Cantwell, G.; Harsch, W. C. *Solid State Commun.* **1998**, *105*, 399−401.

(26) Yagi, E.; Hasiguti, R. R.; Aono, M. *Phys. Rev. B: Condens. Matter Mater. Phys.* **1996**, *54*, 7945.

(27) Zhang, Q.; Dandeneau, C. S.; Zhou, X.; Cao, G. *Adv. Mater.* **2009**, *21*, 4087−4108.

(28) Anta, J. A.; Guillén, E.; Tena-Zaera, R. *J. Phys. Chem. C* **2012**, *116*, 11413−11425.

(29) Memarian, N.; Concina, I.; Braga, A.; Rozati, S. M.; Vomiero, A.; Sberveglieri, G. *Angew. Chem., Int. Ed.* **2011**, *50*, 12321−12325.

DOI: 10.1021/jacs.6b03524
J. Am. Chem. Soc. 2016, 138, 8165−8174

(30) Sobuś, J.; Burdziński, G.; Karolczak, J.; Idígoras, J.; Anta, J. A.; Ziółek, M. *Langmuir* **2014**, *30*, 2505−2512.
(31) Anderson, N. A.; Ai, X.; Lian, T. *J. Phys. Chem. B* **2003**, *107*, 14414−14421.
(32) Chou, T. P.; Zhang, Q.; Cao, G. *J. Phys. Chem. C* **2007**, *111*, 18804−18811.
(33) Tiwana, P.; Docampo, P.; Johnston, M. B.; Snaith, H. J.; Herz, L. M. *ACS Nano* **2011**, *5*, 5158−5166.
(34) Němec, H.; Rochford, J.; Taratula, O.; Galoppini, E.; Kužel, P.; Polívka, T.; Yartsev, A.; Sundström, V. *Phys. Rev. Lett.* **2010**, *104*, 197401.
(35) Selloni, A. *Nat. Mater.* **2008**, *7*, 613.
(36) Grätzel, M. *J. Photochem. Photobiol., A* **2004**, *164*, 3−14.
(37) Nazeeruddin, M. K.; Humphry-Baker, R.; Officer, D. L.; Campbell, W. M.; Burrell, A. K.; Gratzel, M. *Langmuir* **2004**, *20*, 6514−6517.
(38) Vittadini, A.; Selloni, A.; Rotzinger, F. P.; Gratzel, M. *J. Phys. Chem. B* **2000**, *104*, 1300−1306.
(39) Persson, P.; Ojamäe, L. *Chem. Phys. Lett.* **2000**, *321*, 302.
(40) Marcus, R. A. *J. Chem. Phys.* **1956**, *24*, 966.
(41) Tarafder, K.; Surendranath, Y.; Olshansky, J. H.; Alivisatos, A. P.; Wang, L.-W. *J. Am. Chem. Soc.* **2014**, *136*, 5121−5131.
(42) Chu, I.-H.; Radulaski, M.; Vukmirovic, N.; Cheng, H.-P.; Wang, L.-W. *J. Phys. Chem. C* **2011**, *115*, 21409−21415.
(43) Zhang, G.; Canning, A.; Grønbech-Jensen, N.; Derenzo, S.; Wang, L.-W. *Phys. Rev. Lett.* **2013**, *110*, 166404.
(44) Jiang, H.; Blaha, P. *Phys. Rev. B: Condens. Matter Mater. Phys.* **2016**, *93*, 115203.
(45) Tran, F.; Blaha, P. *Phys. Rev. Lett.* **2009**, *102*, 226401.
(46) Ma, J.; Wang, L.-W. *Sci. Rep.* **2016**, *6*, 24924.
(47) Borghi, G.; Ferretti, A.; Nguyen, N. L.; Dabo, I.; Marzari, N. *Phys. Rev. B: Condens. Matter Mater. Phys.* **2014**, *90*, 075135.
(48) Zheng, X.; Cohen, A. J.; Mori-Sánchez, P.; Hu, X.; Yang, W. *Phys. Rev. Lett.* **2011**, *107*, 026403.
(49) Wang, L.-W. *J. Phys. Chem. B* **2005**, *109*, 23330−23335.
(50) McKenna, K. P.; Blumberger, J. *Phys. Rev. B: Condens. Matter Mater. Phys.* **2012**, *86*, 245110.
(51) Shi, L.; Xu, K.; Wang, L.-W. *Phys. Rev. B: Condens. Matter Mater. Phys.* **2015**, *91*, 205315.
(52) Marcus, R. A. *Rev. Mod. Phys.* **1993**, *65*, 599.
(53) Sundararaman, R.; Goddard, W. A., III *J. Chem. Phys.* **2015**, *142*, 064107.
(54) Duignan, T. T.; Parsons, D. F.; Ninham, B. W. *J. Phys. Chem. B* **2013**, *117*, 9421−9429.
(55) Batson, P. E.; Dellby, N.; Krivanek, O. L. *Nature* **2002**, *418*, 617−620.
(56) Siefermann, K. R.; et al. *J. Phys. Chem. Lett.* **2014**, *5*, 2753−2759.
(57) Kamat, P. V. *J. Phys. Chem. Lett.* **2012**, *3*, 663−672.
(58) Koops, S. E.; O'Regan, B. C.; Barnes, P. R. F.; Durrant, J. R. *J. Am. Chem. Soc.* **2009**, *131*, 4808−4818.
(59) Suppan, P. In *Photoinduced Electron Transfer IV*; Mattay, J., Ed.; Springer: Berlin, Heidelberg, 1992; pp 95−130.
(60) Enright, B.; Fitzmaurice, D. *J. Phys. Chem.* **1996**, *100*, 1027−1035.
(61) Oshikiri, M.; Imanaka, Y.; Aryasetiawan, F.; Kido, G. *Phys. B* **2001**, *298*, 472−476.

DOI: 10.1021/jacs.6b03524
J. Am. Chem. Soc. 2016, 138, 8165−8174